Journal of Catalysis 456 (2026) 116729

Contents lists available at ScienceDirect

Journal of Catalysis

journal homepage: www.elsevier.com/locate/jcat

Research article

Alkaline oxide clusters inside zeolites catalyze the selective synthesis of ethyl methyl carbonate

Yongkun Zheng, Nacho Solá-Ferrer, Lluís Martínez-Belenguer, Belén Lerma-Berlanga *, Antonio Leyva-Pérez *

Instituto de Tecnología Química, Universitat Politècnica de València-Agencia Estatal Consejo Superior de Investigaciones Científicas, Avda. de los Naranjos s/n, 46022 Valencia, Spain

ARTICLE INFO

Keywords:
Ethyl methyl carbonate
Oxide clusters
Zeolite
Transesterification reaction
Solid catalysts

ABSTRACT

Ethyl methyl carbonate (EMC), as the simplest asymmetric carbonate, is considered a unique green liquid organic compound for lithium batteries (electrolyte) and gasoline blending (octane enhancer additive), with properties between dimethyl and diethyl carbonate. In accordance, its chemical production is expected to boost during the coming years, despite green chemical syntheses for EMC are still to be developed. Here we show the selective synthesis of EMC from DMC and ethanol with one of the cheapest commercially available solids, i.e. zeolites, as a heterogeneous catalyst for the reaction, surpassing most of the current soluble catalysts employed for this reaction. While a pristine commercial zeolite such as NaX already shows a significant catalytic activity (65% conversion, 91% selectivity to EMC) without any pre-activation treatment, is recoverable and reusable, and can be implemented in batch and in flow, the incorporation of alkaline oxide clusters inside the zeolitic framework, i.e. K_2O, boosts the catalytic activity not only for the NaX zeolite but also for the parent H-USY and NaY zeolites, otherwise barely catalytically active for the reaction, to give yields up to >99% and ≈80% selectivity to EMC. These results bring a sustainable and cheap catalytic system for the production of EMC.

1. Introduction

Nowadays, organic carbonates represent a significant percentage of the worldwide chemical industry. The global carbonate market was valued at $3.5 billion in 2020, and is projected to reach $7.1 billion by 2030 [1]. This is due to the fact that organic carbonates are considered essential components for pharmaceutical [2,3], agrochemicals [4], polymers [5], lubricants [6], electrolytes for lithium–ion batteries [7], solvents for coating [8], varnish [9], and building blocks for chemical reactions [10–13]. In addition, they have been implemented in the energy sector as they lead to better gasoline combustion for reducing emissions [14,15].

Ethyl methyl carbonate (EMC) is a non-symmetric organic carbonate, distinguished because it is environment-friendly, safe-handling (high flash point and low volatility) and low-toxic [16]. These properties make EMC a versatile liquid carbonate with a wide range of applications in different sectors, i.e. as an electrolyte in lithium batteries and as a green additive in gasoline [17]. In accordance, important technological advances have been recently developed for its production, prompted by a market demand which is projected to touch $2.4 billion by 2031. However, the synthetic methods for EMC are still clearly away from the desired sustainability criteria. The synthesis of alkyl carbonates has been traditionally based on the phosgenation reaction of alcohols [18,19], in which the highly toxic and harmful reagents phosgene ($COCl_2$), dimethyl sulfate, pyridine and carbon monoxide are employed (Fig. 1). Phosgene itself is a poisonous gas at room temperature according to the Center for Disease Control (CDC) and one of the most acutely toxic substances used in commerce today and responsible for the chemical industry's worst tragedies [DuPont chemical manufacturing plant (2010) and *Altivia's* petrochemical plant (2023) in United States]. In view of this, new alternative "phosgene-free" syntheses of carbonates have been developed in the last years, which include the oxidative carbonylation of ethanol the combined alcoholysis reaction of CO_2 or urea and the transesterification of carbonates [20]. Most of these reactions have been pushed forward by the convenient use of CO_2 as a raw material, and supported by green chemistry principles (see Fig. 1).

Regarding unsymmetric carbonates, the most developed synthetic routes involve the transesterification of dimethyl carbonate (DMC) with

* Corresponding authors.
E-mail addresses: blerber@itq.upv.es (B. Lerma-Berlanga), anleyva@itq.upv.es (A. Leyva-Pérez).

https://doi.org/10.1016/j.jcat.2026.116729
Received 16 November 2025; Received in revised form 31 December 2025; Accepted 30 January 2026
Available online 2 February 2026
0021-9517/© 2026 The Author(s). Published by Elsevier Inc. This is an open access article under the CC BY-NC-ND license (http://creativecommons.org/licenses/by-nc-nd/4.0/).

different alcohols in the presence of either a homogeneous or a heterogeneous acid or basic catalyst. Catalytic transesterification is one of the most attractive reactions for the synthesis of various esters in terms of atom economy, practicality, substrate generality, and functional group tolerance [21], as showcased by the synthesis of biodiesel after reaction between triglycerides and alcohols, to give an alternative fuel produced from various renewable feedstocks [22].

From the perspective of green and sustainable chemistry, the transesterification of DMC is a convenient reaction since it is based on a feedstock which is considered green and safe, and highly affordable (its open market overcomes 150 kt/year). Therefore, considerable efforts have been invested to developing efficient catalysts for this reaction, as evidenced by the high number of patents licensed [23–25]. Different homogeneous catalysts have been reported for the transesterification of DMC, which include either Lewis or Brønsted acids [26], bases such as K_2CO_3 [27] or TBD (1,5,7-triazabicyclo[4.4.0]dec-5-ene, considered explosive) [28a], and high-valued metal complexes of cobalt [28b] and lanthanoids [28c]. However, all these soluble systems are hardly recoverable and reusable, thus providing a low sustainable process. Inorganic composites such as Mg–La and Mg–Al mixed oxides [29], hydrotalcites [30], CsF/α-Al_2O_3 [31] and α-$KMgPO_4$ [32] have been proposed as solid catalysts, however, some of them require sophisticated and tedious synthetic procedures that get away from green chemistry principles. Metal–organic hybrid materials such as MOFs [33] or the use of enzymes [34] have been also studied to catalyze this reaction, and particularly relevant is the use of basic ionic liquids, poly(ionic liquids) and resins [35], which show high and prolonged-through time catalytic activity and surpass the former [36]. However, the use of such materials is not currently developed for an industrial scale-up.

At this point, the use of much simpler catalysts is worthy to be explored. Surprisingly, perhaps the simpler basic substances in the market which include carbonates, hydroxides and oxide, has barely being reported as catalysts for the synthesis of EMC [37]. In any case, the high basicity of these materials would complicate the control of the transesterification equilibrium, achieving the (bis)trans-esterified product diethyl carbonate (DEC) and making difficult to isolate EMC or to control the grade of purity of the final DMC–EMC–DEC mixture. All this rationale makes one wonder if a very simple micro-structured basic solid could catalyze the transesterification reaction. As said above, EMC holds high value in the current market as it is an excellent candidate as a co-solvent in the electrolyte mixture of commercial lithium-ion batteries, owing to its intermediate physicochemical properties respect to DMC and EDC, thus a massive production is expected in the coming years. In this context, the development of more selective catalysts is crucial, enabling a better control of the reaction while maximizing the value of the resulting products.

The use of porous solids with reticulated channels offers a promising alternative for enhancing the selectivity towards EMC after leveraging the confinement and spatial constraints provided by their structure [38]. EMC has a similar polarity but an intermediate size between DMC and EDC, thus a size or diffusion discrimination is a certain possibility to selectively achieve the desired EMC product. In the present work, we propose the use of widely available basic zeolites as solid catalysts for the reaction. Zeolites are microporous crystalline aluminosilicates that can tune their electronic with the counter cation, in such a way that the acidity of the zeolite frameworks varies from acid (H^+ or Li^+ zeolites) to basic (K^+ or Cs^+ zeolites) [39], and despite acid zeolites had been reported for the transesterification of DMC with very low catalytic activity [39a], we will show here that basic zeolites are very active catalysts. Besides, the channels and cavities of the zeolites can host other basic species such as oxide clusters (K_2O, MgO or CaO), which together with the confinement effect, produce an enhancement of the basic catalysis during the reaction. As a further advantage, the molecular size of the zeolité pores (5–7 Å) could discriminate between the different esterification products of DMC, achieving certain selectivity during the reaction [40]. With this hypothesis in mind, we show in this study the zeolite-catalyzed transesterification of DMC to EMC.

2. Experimental section

2.1. General procedure for the transesterification reaction of dimethyl carbonate (DMC) with ethanol

DMC (84 μL, 1 mmol), EtOH (2 mL, 34.25 mmol) and the desired

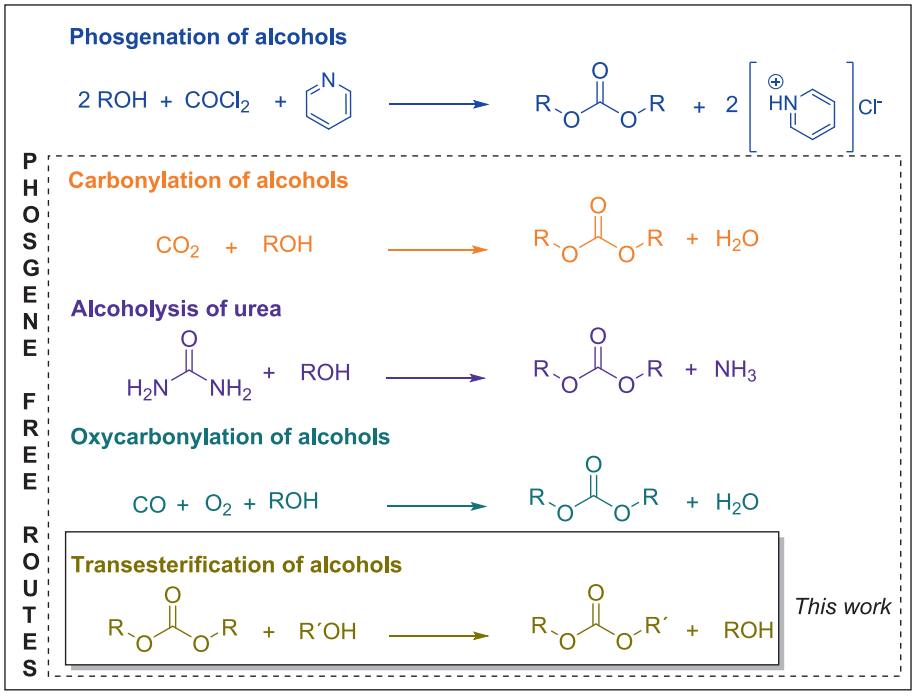

Fig. 1. Synthetic routes for alkyl carbonates. The synthesis route based on the transesterification of alcohols, highlighted within a rectangle, is the one investigated in this work.

amount of catalyst were introduced in a 10 mL vial equipped with a magnetic stirrer. The vial was sealed with a septum, and the resulting mixture was magnetically stirred over a temperature range from 40 to 110 °C on a heating plate for 24 h. The progress of the reaction was monitored by taking aliquots (25 μL) and analysing them by gas chromatography (GC) after dissolving in 1 mL of diethyl ether, filtering through a 25 mm polyamide filter, and adding *N*-dodecane (5.5 μL, 0.025 mmol) as an external standard. The conversion and yields were obtained from calibration curves.

2.2. General procedure for the preparation of ion-exchanged zeolites

The X and Y zeolites in Na^+ form are commercially available. These zeolites were treated with 0.1 M aqueous solutions of KOAc or CsOAc, typically at 70 °C for 24 h, to give the corresponding KNaX and CsNaX zeolites after filtration under vacuum suction and extensive water washings. The extent of this first exchange is typically 65% and 25% for K^+ and Cs^+, respectively. Two more exchanges were carried out in order to increase the total cation exchange to 75% and 36% for K^+ and Cs^+, respectively. The acid zeolites H-USY and ZSM-5 are also commercially available.

2.3. General procedure for the preparation of the hydroxide impregnated zeolites

A cesium hydroxide aqueous solution was incorporated into the zeolite using the incipient wetness impregnation method. Prior to the syntheses, the starting zeolites were activated at 250 °C under vacuum for 16 h. In this method, the adsorbed water in the zeolites pores is removed and only the volume of water necessary to fill back the pores of the zeolite is utilized, ensuring the external surface of the zeolite to remain dry. The CsOH solution (62 mg, 0.37 mmol and 176 mg, 1.05 mmol of CsOH, respectively, dissolved in 0.5 mL of deionized water) was added dropwise to 1 g of NaX zeolite under continuous stirring (with a spatula) to ensure thorough dispersion of the hydroxide throughout the material. Finally, the zeolite was dried at 80 °C overnight. The precise amount of CsOH dissolved corresponds to the desired concentration in the final zeolite. The modified NaX samples were denoted as "n% CsOH@NaX," wherein *n* indicated the weight percentage of CsOH.

2.4. General procedure for the preparation of in situ oxide clusters into the zeolites

Oxide clusters were prepared inside the zeolite by a wet impregnating method followed by a calcination process. As in the previous synthesis, the starting zeolites were activated at 250 °C under vacuum for 16 h. After that, 1 mmol of nitrate salt $M_n(NO_3)\cdot xH_2O$, M = K, Cs, Mg or Ca, was dissolved in the minimum necessary amount of deionized water (typically 0.5 mL). That solution was added dropwise onto 1 g of zeolite. The resulting samples were dried and calcined at 550 °C (ramp: 5 °C·min^{-1}) under a dry air flow for 5 h. The modified zeolite samples were denoted as K_2O, Cs_2O, MgO and CaO@zeolite, respectively.

2.5. Leaching tests

Following the general reaction procedure above, the hot reaction mixture was filtered at intermediate conversion (≈30%), through a 0.25 μm polyamide filter. The filtrates were placed into a new glass reactor equipped with a magnetic stirrer and set at the reaction temperature. The mixture was periodically analyzed by GC, comparing the results obtained with the solid catalyst still in the reaction.

2.6. Typical reaction procedure for reuses

The reuses of the zeolites were performed after separating the solids at the end of reaction by centrifugation and washing three times the solid mixture with ethanol, in order to remove the excess of non-reacted DMC or any product. Subsequently, the zeolite was dried at room temperature overnight and then at 80 °C during 3 h, and directly used in the next reaction.

2.7. In-flow experiments

Dimethyl carbonate (DMC) (**1**) (10 mmol) and ethanol (20 mL, 342 mmol) were placed in a 20.0 mL syringe. The mixture was pumped in counter-gravity mode at atmospheric pressure and at a flow rate of 0.1 / 0.2 / 0.4 mL·min^{-1}, on the bottom of a stainless-steel tube with a 1-inch internal diameter and filled with pelletized NaX (sieved to a particle size of 0.4–0.8 mm). The reaction took place at 110 ℃ and samples were collected by gravity after passing through an U-tube. The samples were analysed by gas chromatography (GC) after dilution of the reaction mixture in a vial with 1 mL of EtOAc, filtering through a 25 mm polyamide filter, and adding *N*-dodecane (5.5 μL, 0.025 mmol) as an external standard. The conversion and yields were obtained from calibration curves.

3. Results and discussion

3.1. Catalytic results for the transesterification of DMC with ethanol with soluble carbonates, oxides and hydroxides

Table 1 shows the catalytic results obtained for the transesterification of dimethyl carbonate (DMC) (**1**) with ethanol (0.5 M) at 110 °C for 24 h, using different soluble inorganic salts. The reactions were followed by gas chromatography (GC) and the structure of the well-known products ethyl methyl carbonate (EMC) (**2**) and diethyl carbonate (DEC) (**3**) were confirmed by mass spectrometry (GC–MS) and also by comparison with pure samples. It is worthy to comment here that the transesterification reaction is an equilibrium that, without in-situ removal of the products, can go back at a certain conversion, which in the case of DMC (**1**) with ethanol is typically located ≈70% conversion at 80–110 °C [41]. Only extremely active catalysts can push the equilibrium towards the products without in-situ product extraction (i.e. by reactive distillation) [42].

As it can be seen in Table 1 (entry 1), the reaction does not occur in the absence of a catalyst, even at 110 °C. In contrast, the reaction works in the presence of carbonates [27] (entries 2–5), to give a variety of conversions. K_2CO_3 [27] and $MgCO_3$ show the best results, obtaining full conversions after 24 h of reaction and total selectivity for product DEC (**3**) (entries 2 and 4). However, Cs_2CO_3 did not give a significant conversion and $CaCO_3$ gave an intermediate conversion with good selectivity toward EMC (**2**) (entries 3 and 5, respectively). When different metal oxides were employed (entries 6–11), low conversions were obtained. Among these, the CaO shows a moderate conversion of 42% after 24 h of reaction, a similar result to $CaCO_3$. Alkaline earth hydroxides (entries 12–15) give excellent conversions and good selectivity to DEC (**3**) at 110 °C, after just 2 h of reaction and with much lower amounts of catalyst (0.08 mol%). Unfortunately, the transesterification reaction gets uncontrollable and a poor selectivity towards EMC (**2**) is observed. Kinetic studies of the transesterification reaction under these low catalytic loadings and at lower temperatures were then carried out in order to stop the reaction at the desired EMC (**2**) product (for more details, see Tables S1–S2 and Fig. S1 in Section 1 in the Supporting Information, SI). The alkaline earth hydroxides prove their high activity even at 40 °C, particularly CsOH, which showed >99% conversion with just 0.08 mol % of catalyst. The activity trend is in accordance with the intrinsic basicity of each hydroxide (Fig. S2), thus we can conclude that a higher basicity is beneficial for the transesterification of DMC (**1**) with EtOH, probably because the basic sites activate ethanol to enhance its nucleophilicity through transient ethoxy ($EtO^{\delta-}$) species [43]. Moreover, a decrease in the amount of catalyst enables a certain control towards the formation of the EMC (**2**) product. To the best of our knowledge, these

Table 1
Results for the transesterification reaction of DMC (**1**) with ethanol, catalyzed by different inorganic salts (14.5 mol%) after 24 h of reaction at 110 °C. GC yields.

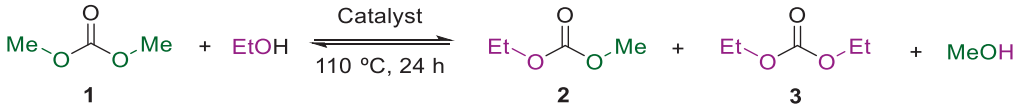

1 **2** **3**

Entry	Catalyst	Conv. of DMC (**1**) (%)	Selectivity (%)	
			EMC (**2**)	DEC (**3**)
1	None	<2	100	–
2	K_2CO_3	>99	8	92
3	$CsCO_3$	4	100	–
4	$MgCO_3$	>99	8	92
5	$CaCO_3$	59	92	8
6	MgO	24	96	4
7	CaO	42	80	20
8	ZnO	16	100	–
9	CuO	<5	100	–
10	Al_3O_2	35	97	3
11	ZrO_2	9	100	–
12	NaOH[a]	>99	7	93
13	KOH[a]	>99	8	92
14	CsOH[a]	>99	7	93
15	CsOH[b]	>99	9	91

[a] Reaction time 2 h.
[b] Catalyst 0.08 mol%.

results, as a whole, illustrate for the first time the use of KOH and CsOH as potential catalysts for the transesterification reaction of DMC (**1**), with TOF values of 1094 h^{-1} and 1906 h^{-1}, respectively (see Table S3).

3.2. Catalytic results with zeolites

3.2.1. Zeolite NaX

Based on the above results, basicity plays a crucial role in the activity of the catalyst during the transesterification reaction of DMC (**1**). However, none of the inorganic oxides exhibited an intrinsic selectivity towards the formation of EMC (**2**) beyond the thermodynamic control of the transesterification equilibrium. Therefore, to achieve control over the reaction selectivity, the use of porous reticular framework materials was considered to control the selective formation of EMC (**2**) through the size of their pores and channels. Here we propose a detailed study of the transesterification reaction using a series of zeolites with basic characteristics, the commercially available NaX and its post-synthetically modified counterparts. For that, we chose zeolite NaX (12 MR), since it is a crystalline tridimensional microporous aluminosilicate which easily coordinates metal cations within pores of 7.4 Å size, thus allows us good accessibility of the reagents to the catalytic centers and a good diffusion out of the products [40]. This zeolite displays a low silicon/aluminium molar ratio, close to unity (Si/Al = 1.2), and this higher aluminium content means an increase in the number of active basic centers, thus improving the basic properties of the zeolite, to make it a potential catalyst for the transesterification reaction. As control experiments, a range of commercially available zeolites with acidic or neutral properties and different pore diameters were also evaluated, including H-USY (ultra-stabilized Y acid zeolite), NaY, H-BETA (12-MR), H-ZSM-5 (10-MR), and A-5 (8-MR). The catalytic results for the zeolitic materials are included in Table 2. A 5 wt% amount of zeolite was employed, which might be suitable for high-scale implementation [44].

The results in Table 2 confirm the low activity of the acid zeolites (entries 1–3), in good accordance with the literature [39a]. The remarkably high activity of the H-BETA zeolite is notable, which poses challenges in achieving precise control over its selectivity (entry 4). In contrast, zeolite NaX shows a good catalytic activity for the transesterification reaction, with a good conversion (65%) and an excellent selectivity towards EMC (**2**) (91%, entry 6). It is important to emphasize here again that the transesterification of DMC (**1**) is an equilibrium

Table 2
Catalytic results of the transesterification reaction of DMC (**1**) with ethanol (0.5 M) with different zeolites (35 mg, 5 wt% in the mixture) after 24 h of reactions. GC yields.

Entry	Catalyst	Conv of DMC (**1**) (%)	Selectivity (%)	
			EMC (**2**)	DEC (**3**)
1	A–5	<1	–	–
2	H–ZSM–5	22	92	8
3	H–USY	22	92	8
4	H–BETA	>99	8	92
5	NaY	8	100	0
6	**NaX**	**65**	**91**	**9**
7	KNaX	<5	100	–
8	CsNaX	<5	100	–
9	NaX (activated at 250 °C)	<5	100	–
10	KNaX (activated at 250 °C)	<1	–	–
11	CsNaX (activated at 250 °C)	<1	–	–

reaction, so to achieve conversions significantly beyond 70%, techniques such as reactive distillation would be necessary in most cases. Therefore, the catalytic result obtained with zeolite NaX is remarkable and, indeed, a kinetic experiment showed that a quantitative conversion of DMC (**1**) can be obtained but at expenses of the selectivity to EMC (**2**) (50%, Fig. 2a). In any case, if we compare these results with those obtained using the soluble inorganic oxides employed in Table 1, we see that the nanostructure of the zeolite channels exerts some control over the formation of the intermediate compound, at least under the selected catalytic conditions. If this is so, more basic zeolites where the molecular diffusion is much restricted due to the bigger size of the introduced alkaline-earth counteraction [39c], such as KNaX and CsNaX, might not catalyze the reaction. To test this hypothesis, we modified the basicity of the commercial zeolite NaX by ion exchange with alkali metal cation solutions [45]. In this way, the overall basicity of zeolites should increase with more electropositive alkali cations ($Na^+ < K^+ < Cs^+$), as explained by Sanderson's intermediate electronegativity model [46a,b]. Inductively coupled plasma-atomic emission spectroscopy (ICP-AES, Table S3) confirmed the partial exchanged of cations in the NaX structure, reflecting that the size of the K^+ cation promotes the higher degree

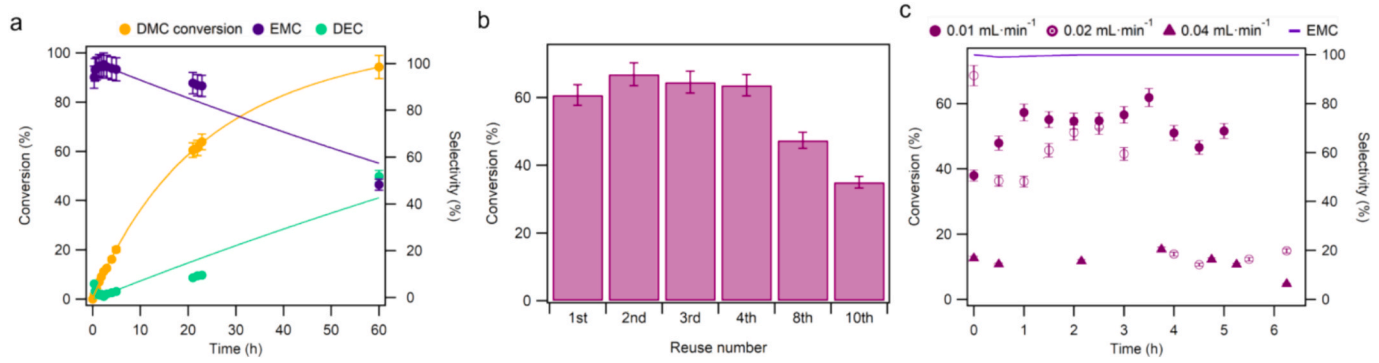

Fig. 2. a) Kinetic profile for the transesterification reaction of dmc (**1**) with ethanol catalyzed by NaX (35 mg) at 110 °C. b) Recyclability study of the zeolites NaX in the transesterification reaction of DMC with ethanol (0.5 M) at 110 °C. c) In–flow reaction with pelletized NaX zeolite as a catalyst (35 mg) for the transesterification reaction of DMC (**1**) with ethanol (0.5 M) at 110 °C. Different feed flow rates were evaluated. Error bars account for a 5% uncertainty. Conversions and selectivity were calculated by GC, using *N*–dodecane as an external standard.

of cation exchange respect to bigger Cs^+ cation. Fourier transformed infrared spectroscopy (FT-IR, Fig. S4) and powder X-ray diffraction (PXRD, Fig. S4) measurements confirm the integrity of the zeolites after the exchange procedures. The internal vibrations of the framework's TO_4 tetrahedra of the zeolite are insensitive to variations in the framework electronics, but the external linkages between tetrahedra can be affected by the electron density, thus the basicity of the zeolite. To check this, a further analysis of the FT-midIR spectra (1300–200 cm^{-1}) of the zeolites was carried out, and the spectra (Fig. S5 and Table S5) shows that the bands associated to the double ring (DR_6) vibrations and to the T–O bending modes in tetrahedra, centered in zeolite NaX at 560 and 447 cm^{-1}, respectively, shift to lower wavenumbers for KNaX and CsNaX (544/437 and 557/445 cm^{-1}, respectively), in line with a higher basicity of the zeolite framework for the latter. The catalytic results with the KNaX and CsNaX zeolites barely show any conversion (entries 7–8), which indicates that a suitable balance between basicity and molecular diffusion is required for the zeolite to catalyze the reaction [46c–e]. Besides, the drying of the NaX zeolite catalysts at 250 °C under vacuum led to a complete loss of the catalytic activity (entries 9–11), which strongly supports the active role of adsorbed water during reaction. The analysis of these results indicate a trade-off between the zeolite pore size and its basicity, providing further insight into the structure–activity relationships governing the selective synthesis of EMC. Table SX compiles these results along with the key characteristics of each zeolite, offering a comprehensive overview.

Given the promising catalytic results with the NaX zeolite, the next step was to evaluate the recyclability of the catalyst. The recyclability study of the zeolite shows that it can be used up to 10 times while maintaining a reasonable catalytic activity [≈40% yield of (**2**) in the tenth use (Fig. 2b)]. A hot filtration test was then carried out in order to evaluate the possible presence of catalytically active species in solution. The test revealed that, after filtering the zeolite NaX catalyst off at 10% conversion, the formation of the EMC products (**2**) is severely stopped, accounting for an 8% of the total yield of the reaction (Fig. S6). ICP analysis after successive uses reveals a slight decrease in the Si/Al ratio (Table S7), which might correlate with the partial loss of catalytic activity. A desilication process, likely caused by attack of the reactants (EtOH and DMC) on the Si–O–Al bonds, might lead to the formation of extra-framework aluminum species and framework defects. Although the intrinsic basicity of the material increases, as indicated by FT-IR analysis (see Fig. S7), these structural changes redistribute compensating Na^+ cations and distort the zeolite framework, reducing the accessibility of the basic sites. As a result, the effective basicity decreases, leading to a progressively loss of conversion in the transesterification reaction over consecutive runs.

Building upon these results, we decided to go one-step further and evaluate the value of the NaX zeolite catalyst under in-flow reactions conditions. For this experiment, different flow rates were tested, as shown in Fig. 2c. The results suggest that a relatively low flow rate of 0.01 $mL{\cdot}min^{-1}$ enables moderately high conversions, very close to the equilibrium, which remain constant over time. However, increasing the flow rate leads to a marked decrease conversion of DMC (**1**). Notably, a complete selectivity for the formation of the desired product EMC (**2**) was observed across the three experiments conducted, corroborating the specificity of the NaX zeolite catalyst for EMC (**2**) production.

3.2.2. *Hydroxide impregnation*

With the above results in hand, we decided to support cesium hydroxide CsOH in NaX zeolite, since the former is extremely active for the transesterification reaction and the latter might be able to isolate and stabilize the CsOH active species, to improve the recyclability of the catalyst. In a first approach, CsOH was incorporated in the solid by the wetness impregnation method, since impregnated zeolites with basic hydroxides are known in the literature [48]. Two different loadings (6 and 18 wt%, see Section 2.2. in the SI for synthetic details) were employed, and the resulting solids were denoted as 6%CsOH@NaX and 18%CsOH@NaX, respectively. The new solids were characterized by FT-IR and PXRD (Figs. S8–S9), confirming the integrity of the faujasite zeolite crystallinity and ruling out any phase transformation after CsOH incorporation [47]. It is worth notice that the impregnated zeolite NaX, with Cs^+ hydroxides, does not present such a steric hindrance as the CsNaX zeolite, since the amount of reported Cs^+ cations are lower for the former.

The 6%CsOH@NaX and 18%CsOH@NaX solids were then tested as catalysts in the transesterification reaction of DMC (**1**), under the optimized reaction conditions for zeolite NaX (see, for instance, Table 2 above, entry 1), and their catalytic activity was compared with the commercial zeolite NaX. The results (Table S8) evidence a much higher catalytic activity of the CsOH@NaX zeolites. Kinetic experiments with 6% and 18%CsOH@NaX showed that almost total conversion was achieved after just 4 h and 1 h, respectively (Fig. S10), but while the selectivity to EMC (**2**) was low even at moderate conversions for the most loaded CsOH zeolite, a significant selectivity to EMC (**2**) was obtained at high conversions with 6%CsOH@NaX as a catalyst (77% selectivity at 82% conversion). This result was obtained after just 90 min reaction time, which supposes 20 times less time than that required to achieve the same result with the pristine NaX zeolite (30 h, see Fig. 2a). Indeed, an initial rate acceleration of 20 and 45 times for 6%CsOH@NaX and 18%CsOH@NaX, respectively, was observed (Fig. S11). Unfortunately, a hot filtration test at 30% did not show any significant

difference between the reaction with and without catalyst (Fig. S12), which denotes the presence of CsOH in solution.

3.2.3. *In situ formation of oxide clusters*

The previous results suggest that the transesterification reaction is responsive to basic species supported into the zeolite channels. Therefore, the next approach was to investigate alternative methods to increase the basicity of the framework without compromising the sterics of the zeolite and minimizing the leaching. In this context, we envisioned the incorporation of metal alkali clusters and small oxide particles onto the NaX zeolite. For the sake of comparison, we also studied the NaY zeolite, which is completely inactive for the catalytic reaction but has the same type of structure and pore size of NaX; the main difference is the Si/Al ratio, i.e. 1.2 for NaX and 2.5 for NaY. In order to generate the ultrasmall oxide aggregates into the zeolite, reported procedures [49,50] were followed, which involved the impregnation of the zeolite with an aqueous solution of different nitrate salts [$M(NO_3)_n$, M = K, Cs, Mg, Ca) and then a calcination process at 550 °C, for 5 h under dry air flow (see Section 2.3 in the SI for further details). The new series of catalyst denoted as (K_2O, Cs_2O, MgO, CaO)@NaX/Y, respectively, were characterized by ICP-AES, FT-IR, PXRD and TEM, to compare with the hosting zeolites. The ICP-AES results confirm the incorporation of the additional metal (Table S9), while the FT-IR spectra of the catalytic solids show the characteristic bands of the pristine zeolites [51] (Fig. S13) and the PXRD diffractograms show that the new solids are isostructural and as crystalline as the commercial NaX and NaY zeolites (Fig. S14). The only exception was Cs_2O@NaX, which shows a small loss of crystallinity after wet impregnation and calcination, probably due to the large size of the Cs^+ cations. This might be related with the failure of the reaction (CsNaX) or the leaching (CsOH@NaX) when Cs^+ zeolites were employed as catalysts. In any case, the diffraction lines related to the phase of the metal oxides could not be distinguished, indicating that the supported oxides are in sub-nanometric form [52].

An analysis of the midIR area was carried out to assess if the new (K_2O, Cs_2O, MgO, CaO)@NaX/Y zeolites have increased or not their framework electronic density. Fig. 3a shows that the peaks centered at 560/447 cm^{-1} for NaX remains virtually unchanged, if not somewhat shifted (+1–2 cm^{-1}) (see Table S10). The same occurs with the NaY zeolite (Fig. S15 and Table S11). These results indicate that the oxide clusters formed inside the NaX and NaY zeolites do not modify the intrinsic basicity of the original zeolite. An exceptional noteworthy change is observed in the Si–O–M band centered at 665 cm^{-1} for MgO@NaX; in this case, the peak shifts towards higher wavenumbers, which may suggest that some of the framework Na^+ ions have been exchanged for similarly sized Mg^{2+} cations.

X-ray photoelectron spectroscopy (XPS) measurements were carried out to further characterize the clusters into the zeolites (Figs. S16–S23). As illustrated in Fig. 3b, the samples show the appearance of two differentiated O 1*s* binding energies at ≈532.0 and ≈534.0 eV in all cases, which correspond to the expected Si–O–Al bonds in the zeolite framework and the cluster oxide signals, respectively [39c]. These results confirm the presence of the oxide clusters in the NaX and NaY zeolite framework.

In addition, a comprehensive analysis was performed using several electron microscopic techniques to confirm the cluster nature and their location in the zeolites. It should be noted that the direct observation of such alkali clusters in zeolites is often challenging due to their chemical nature. In many cases (e.g., K, Mg, Ca), the metal density is insufficient to clearly distinguish them from the zeolite framework elements (Na, Si, Al), or they may reside within the zeolite interior and be very small, as is

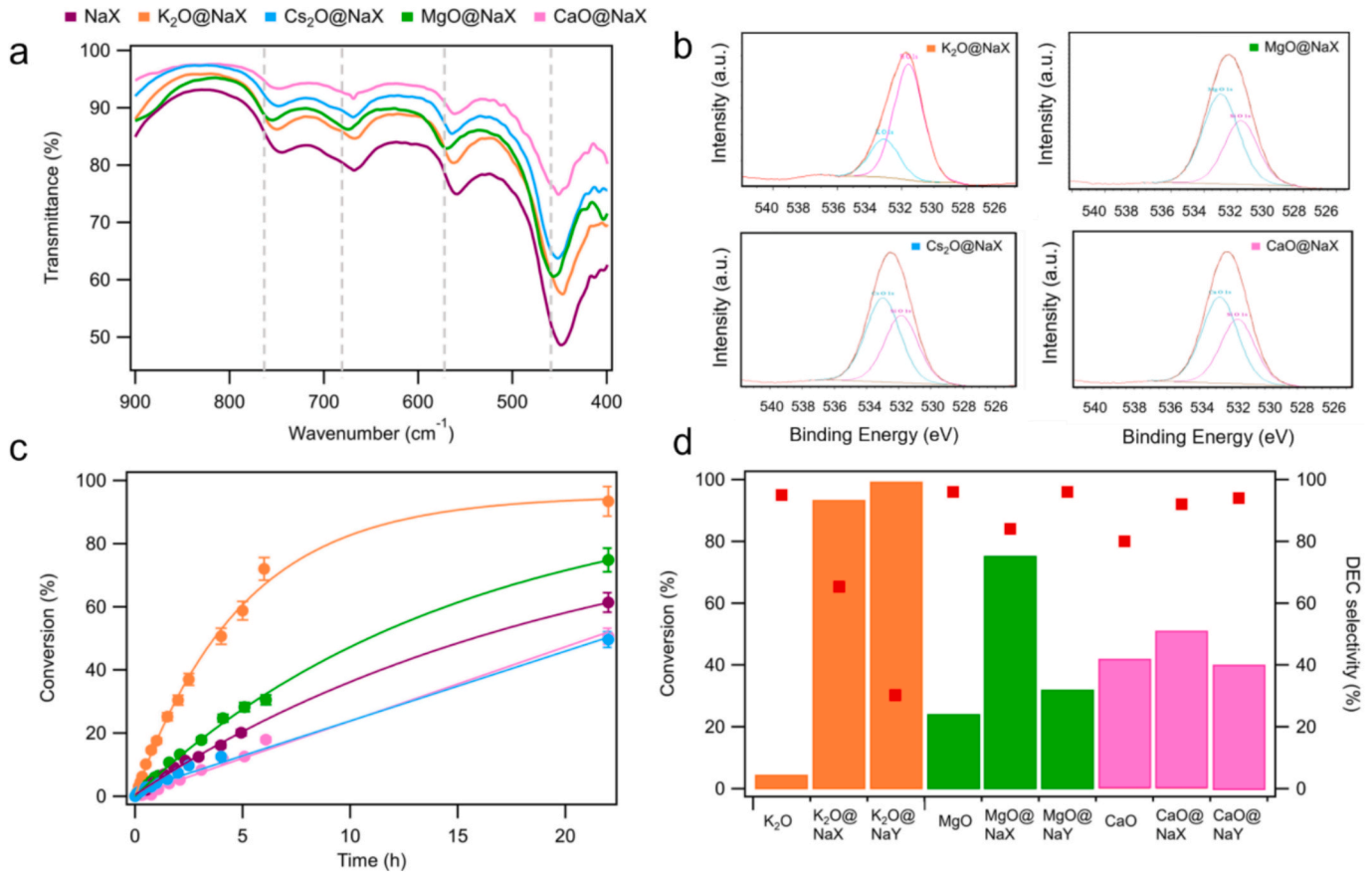

Fig. 3. a) Zoom of the FT–midIR spectra (900–400 cm^{-1}) for MOx@NaX zeolites. b) O *1 s* X–ray photoelectron spectra (XPS) for MOx@NaX zeolites c) Kinetic profile for the transesterification reaction of DMC (1) with ethanol (0.5 M) catalyzed by MOx@NaX zeolites (35 mg) at 110 °C (the colour lines correspond to those in Figure a). Error bars account for a 5% uncertainty. d) Comparison of catalytic results of MOx@NaX/Y zeolites and the corresponding oxides.

the case in our study. Bright field-scanning transmission electron microscopy (BF-STEM) images (Fig. S24) do not show any regions of increased brightness on the sample surface, thus ruling out the presence of potassium aggregates on the surface. Furthermore, EDX mapping analysis also confirms a homogeneous distribution of K throughout the crystal (Figs. S25 and S26). To further investigate the interior of the crystals and confirm the presence of metal oxide clusters within the zeolite, the Cs_2O@NaX sample was analyzed, as the higher atomic number of Cs facilitates its detection. First, the surface of the sample was examined. High-angle annular dark-field-scanning transmission electron microscopy (HAADF-STEM) images (Fig. S27) rule out the presence of surface aggregates, as observed in previous samples, and reveal a homogeneous distribution across the crystal. Subsequently, a cross-section of the crystal was prepared by focused ion beam-scanning electron microscope (FIB-SEM) and analyzed by HAADF-HRSTEM (Fig. S28) and EDX mapping (Fig. S29), showing a uniform distribution of Cs and the absence of aggregates. These observations indicate that the clusters are located inside the zeolite crystal. However, their nanometric size prevents direct visualization due to the resolution limits of the instruments. Based on the analysis of these two samples, this information can be extrapolated to the other zeolites prepared in this study, as the cavity sizes are similar and the synthesis procedures are identical. Overall, the combined results obtained from the applied characterization techniques strongly support the presence of nanometric alkali oxide clusters within the zeolite framework.

Table 3 presents the catalytic results with the *in situ*-formed oxide clusters in the zeolite; it can be observed that, for the case of impregnated and calcinated NaX zeolite (entries 1–4, see Fig. S30 for the kinetic profiles), the *in situ* formation of Cs and Ca oxides does not improve the catalytic activity of the original zeolite (entries 2 and 4), but the formation of MgO oxide increases the conversion of DCM (**1**) up to 75% with a 84% selectivity to EMC (**2**) (entry 3), and the catalytic performance given by K_2O@NaX is remarkable, obtaining a 93% conversion after 24 h, with a 65% selectivity (entry 1). This exceptionally high result is even beyond the equilibrium mixture without any reactive distillation required, probably enable by the steric discrimination of the K_2O@NaX zeolite framework.

Fig. 3c shows the kinetic profiles for the different (K_2O, Cs_2O, MgO, CaO)@NaX catalysts, where the higher activity of the supported K_2O and MgO clusters is clearly visualized. These changes are also manifested in the initial reaction rates (see also Fig. S25 and Table S12). Here, importantly, the selectivity to EMC (**2**) increases significantly at higher conversions, to obtain yield up to 63% with MgO@NaX. The stability of Ca and Mg oxides enable to compare the catalytic activity of the bulk oxides with the species generated in the zeolite (Fig. S31). In the case of CaO, any improvement is not observed when the oxides particles are generated *in situ* in the zeolite. In contrast, MgO@NaX is catalytically superior to the corresponding unsupported MgO counterpart, and particularly striking is the case of K_2O. The latter was prepared from KNO_3 by employing the same thermal procedure but without the zeolite (heating at 550 °C for 5 h), which allowed us to obtain a solid to precisely compare the K_2O@NaX material with its corresponding bulk oxide. The results for calcined KNO_3 were poor, showing a conversion below 4% (see Fig. S32). These results highlight the value of NaX zeolites in generating the chemical microenvironment to support the oxide clusters, which, in principle, are not formed or isolated outside the zeolites cavities. In the case of NaY zeolite, a considerable increase in catalytic activity is observed for all the oxide cluster analogues (entries 5–8 in Table 3) compared to the pristine zeolite (Table 2, entry 1). These results indicate that the intrinsic basicity of the clusters is responsible for the observed activity; similar to the behaviour seen in K_2O@NaX, the K_2O@NaY material achieves the best results. However, in this latter case, a slight decrease in selectivity towards EMC (**2**) was observed (see Fig. 3d for a direct comparation).

Table 3
Catalytic results for the transesterification reaction of DMC (**1**) with ethanol (0.5 M) catalyzed by different zeolites (35 mg) after 24 h of reactions at 110 °C. GC yields.

Entry	Catalyst	Conv. of DMC (1) (%)	Selectivity (%)	
			EMC (**2**)	DEC (**3**)
1	K_2O@NaX	93	65	35
2	Cs_2O@NaX	50	92	8
3	MgO@NaX	75	84	16
4	CaO@NaX	51	92	8
5	K_2O@NaY	99	30	70
6	Cs_2O@NaY	96	51	49
7	MgO@NaY	32	96	4
8	CaO@NaY	40	94	6

In order to further confirm the direct relationship between the K_2O cluster basicity and the increased activity observed in the K_2O@NaX zeolite, CO_2 was employed as an acid probe in in-situ FT-IR experiments. For this purpose, CO_2 adsorptions were performed in the pristine NaX zeolite and K_2O@NaX, and both the physisorption region (2400–2200 cm^{-1}) and the chemical adsorption region of CO_2 (1800–1200 cm^{-1}) were independently evaluated. In the former region, the bands correspond to the antisymmetric ν_3 modes of physisorbed CO_2 and CO_2 linearly adsorbed on cationic sites (CO_2–Na^+, CO_2–Mg^{2+}, etc.) can be differentiated, since the polarization power of the cation causes shifts towards higher frequencies in the CO_2 absorption band. Meanwhile, in the chemical adsorption region, adsorbed species such as bicarbonates (HCO_3^-), unidentate, bidentate, and tridentate carbonates (CO_3^{2-}), free carbonates, and carboxylates can be observed.

The analysis of the physisorption region (Fig. S33) shows that, at low doses, a broad band centered at 2355 cm^{-1} is observed in the NaX zeolite, which increases when rising the CO_2 pressure. This band shows a hypsochromic shift in the case of the K_2O@NaX zeolite, now appearing at 2350 cm^{-1}, indicating a stronger interaction of CO_2 with the basic centers, suggesting that the K_2O@NaX zeolite possesses more basic sites. In addition to this band, the emergence of a new band centered at 2286 cm^{-1} is detected at higher CO_2 pressures, and this band is attributed to CO_2 linearly adsorbed on cationic sites (Na^+). These values align well with those reported for other zeolites with similar structures [53] and strongly suggest that the K_2O clusters are acting independently of the NaX zeolite framework.

Fig. 4 shows the FT-IR chemisorption region for CO_2 in the NaX and K_2O@NaX zeolites. To better analyze the formation of new bands associated with species formed in the presence of CO_2, the spectra for both zeolites were compared under vacuum and in the presence of a high

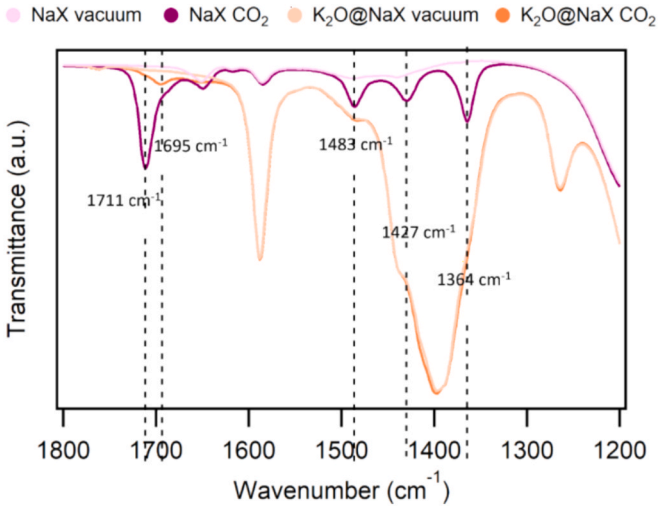

Fig. 4. FT–IR spectra of NaX and K_2O@NaX zeolites in vacuum and obtained after adsorption of CO_2 at 25 °C in the CO_2 chemisorption region (1800–1200 cm^{-1}).

concentration of CO_2. In the case of the NaX zeolite, the adsorption of CO_2 is determined by the appearance of two pairs of bands at 1711 which remains after heating at 100 °C, and 1364 cm^{-1}, and at 1483 and 1427 cm^{-1}, as previously reported [53]. The two lower-frequency pairs correspond to the symmetric and asymmetric stretching modes of unidentate carbonates, while the bands at 1710 and 1360 cm^{-1} can be associated with the formation of polydentate carbonate species. For the zeolite containing the K_2O cluster, the analysis is more complex, as several of these bands are overlapped by higher-intensity bands that can be attributed to K_2O vibrations (a broad band centered around 1400 cm^{-1}). However, the higher wavenumber region, attributed to the vibrations of unidentate carbonates, can still be differentiated. In this region of the spectrum, a shoulder at 1711 cm^{-1} can be observed for the K_2O zeolite, along with the formation of a new, more intense band at 1695 cm^{-1} and additional band appears at 1652 cm^{-1}, which remains after heating the sample to 100 °C (see also Fig. S33). The presence of these species suggests that the framework of the K_2O@NaX zeolites combines the basicity contribution of the original zeolite with the new basicity arising from the presence of the basic cluster, in good agreement with the FT-IR results for the CO_2 physisorption region and the zeolite framework. Indeed, a certain correlation between catalytic activity and the basicity of the zeolites can still be observed [54].

Given the favourable results for the K_2O@NaX material [high conversions and significant selectivity towards EMC (**2**)], we conducted reusability studies for the transesterification reaction. First, a hot filtration test was performed in order to evaluate whether the catalytically active species remain or not in the solid during reaction, and the results show that, despite some leaching of K_2O occurs, the catalytic activity in the solid accounts for >50% even in a hot polar solvent such as ethanol (Fig. S35). In good agreement with this, the ICP analysis reveals that the K content in the sample remains at least to the half after its fourth use (Table S13). To diminish this leaching, the reaction conditions were slightly modified by replacing part of the ethanol with toluene, a less polar and less lixiviating solvent. A 1:1 ethanol:toluene mixture was selected and subsequently applied in the transesterification experiments. Under these conditions, leaching was completely eliminated (Fig. S36 and Table S13). These results indeed open the way to use zeolites as true solid catalysts for the synthesis of EMC (**2**) by transesterification reaction of DMC (**1**) with ethanol.

Going one step further and following the rationale above, we envisioned that the incorporation of the basic MO_x clusters into acidic (H-USY, H-ZSM-5 and H-BETA) rather than neutral or basic zeolites might allow the generation of catalytic active materials that combine Lewis acidic and basic centers within a given proximity, which may be optimal for forming Frustrated Lewis Pairs (FLP) and enhancing the catalytic potential of the zeolitic material [55]. Please notice that the H-USY zeolite is low active for the transesterification reaction (22%, Table 2, entry 3). However, after incorporating the different oxide clusters by the same protocol than for NaX and NaY zeolites, the materials (K_2O, Cs_2O, MgO, CaO)@HUSY catalysts became highly catalytic active (Table S14), with even better results than the corresponding NaY-hosting cluster oxides (compare with Table 3, entries 5–8). The CaO@HUSY zeolite showed the better balance between DMC (**1**) conversion (70%) and EMC (**2**) selectivity (92%) under the optimized reaction conditions. The comparison of the catalytic activity of our materials with previously studied catalysts (see Table S15) highlights their outstanding performance, positioning them among the most efficient systems reported. ICP-AES, FT-IR and PXRD analyses confirm the formation of oxide clusters and the stability of the zeolites' framework (Table S15 and Figs. S37–S43) The FT-IR analysis of the materials also show that the bands associated to the double ring (DR_6) vibrations and to the T–O bending modes in the tetrahedra of the H-USY zeolite (525 and 453 cm^{-1}, respectively) remain practically unshifted after the incorporation of the cluster oxides (Fig. S44 and Table S16), which indicates that the acidity of the H-USY zeolite is not modified by the presence of the clusters.

Pyridine adsorption FT-IR experiments confirmed that the intrinsic acidity of the zeolite framework remained intact, enabling the coexistence of Brønsted and Lewis acid sites, since the bands at ~1540 and ~1635 cm^{-1} assigned to pyridinium ions and the bands at ~1455 and ~1620 cm^{-1} assigned to Lewis sites, typically associated with extra-framework Al species (see Fig. S44), were both found in the K_2O@H-USY material. Notably, the bands related to Lewis sites exhibit a red-shift to lower wavenumbers, suggesting a stronger interaction with pyridine and an increased electron-accepting ability of these centers. This effect may arise from a higher local positive charge on the Al centers or a more confined environment within the zeolite pores, indicating not only preserved acidity but also enhanced Lewis acidity in the modified catalyst. XPS measurements show the expected signals for the clusters and the zeolite framework, however, the different O 1*s* binding energies could not be differentiated as in the case of the NaX and NaY zeolites since the H-USY zeolite can show a higher Si–O–Al bonding energy (Figs. S34–S37), near to the oxide clusters. In any case, these results showcase the persistence of basic alkaline oxide clusters inside the acid faujasite zeolites, with enhanced catalytic activity, in both basic and acid zeolite frameworks.

4. Conclusions

The selective transesterification of DMC (**1**) with ethanol to EMC (**2**) is catalyzed by simple basic salts (i.e. CsOH) and zeolites (i.e. NaX) with higher activity that many previously reported catalysts. For instance, the commercially available NaX zeolite produces EMC (**2**) in moderate yield (65%) but very good selectivity (91%), without any pre-treatment required, reusable up to ten times, and implemented in batch and in-flow. However, the incorporation of oxide clusters, particularly K_2O and Cs_2O, into the zeolite framework significantly enhances the catalytic activity of NaX, achieving EMC yields above 60% and conversions exceeding 90% in the case of K_2O. The enhancement is even more pronounced for zeolites that are intrinsically inactive, as the introduction of alkali oxide species—especially K_2O and Cs_2O—into NaY and H-USY zeolites enhances significantly the catalytic activity (up to 99% conversion, beyond the equilibrium point without any reactive distillation). Notably, CaO@HUSY achieves a high EMC selectivity of 92% while maintaining a conversion of 70%. In the case of H-BETA zeolite, the presence of K_2O clusters improves selectivity, leading to an EMC yield of 63%. A combined analysis (kinetics, in-situ FT-IR, PXRD, XPS, EA and electron microscopy techniques) of the prepared solids provides insights into the origin of the basicity, allowing for its correlation with the observed catalytic activity. These results open the way to design zeolite catalysts for the selective production of EMC (**2**) by transesterification reaction of (**1**) and, by extension, for other transesterification reactions.

CRediT authorship contribution statement

Yongkun Zheng: Writing – original draft, Methodology, Investigation, Formal analysis. **Nacho Solá-Ferrer:** Writing – original draft, Methodology, Investigation, Formal analysis. **Lluís Martínez-Belenguer:** Writing – original draft, Methodology, Investigation, Formal analysis. **Belén Lerma-Berlanga:** Writing – original draft, Supervision, Methodology, Investigation, Formal analysis, Conceptualization. **Antonio Leyva-Pérez:** Writing – original draft, Supervision, Investigation, Funding acquisition, Formal analysis, Conceptualization.

Declaration of competing interest

The authors declare that they have no known competing financial interests or personal relationships that could have appeared to influence the work reported in this paper.

Acknowledgements

We thank the Ministerio de Ciencia e Innovación Spain (MICIIN) for grant numbers PID2023-148441NB-I00 and Severo Ochoa Program CEX2021-001230-S. Y.Z. thanks to the China Scholarship Council (CSC No: 202009350009). B.L.-B. thanks a Juan de la Cierva grant (JDC2022-048323-I). Ll. M.-B. thanks the Severo Ochoa program for the concession of a contract.

Supporting information

Additional experimental details, Figs. S1–S38 and Tables S1–S2, divided in five sections, can be found as Supporting Information.

Appendix A. Supplementary data

Supplementary data to this article can be found online at https://doi.org/10.1016/j.jcat.2026.116729.

Data availability

Data will be made available on request.

References

[1] D. Fuller, Carbonate Market Report 2024 (Global Edition), Cognitive Market Researck, USA, 2023. Global Ethyl Methyl Carbonate Market Insights and Forecast To 2032 (Global Edition), Business Research Insights, India, 2023. https://www.businessresearchinsights.com/market–reports/ethyl–methyl–carbonate–market–107348.
[2] H. Zhang, M.W. Grinstaff, J. Am. Chem. Soc. 135 (2013) 6806–6809.
[3] S.E. Anderson, J. Franko, K.L. Anderson, A.E. Munson, E. Lukomska, B.J. Meade, J. Immunotoxicol. 10 (2013) 59–66.
[4] G. Kuriakose, J.B. Nagy, N. Nagaraju, Catal. Commun. 6 (2005) 29–35.
[5] J.H. Park, J.Y. Jeon, J.J. Lee, Y. Jang, J.K. Varghese, B.Y. Lee, Macromol 46 (2013) 3301–3308.
[6] A.S. Pensado, A.A.H. Pádua, M.J.P. Comuñas, J. Fernández, J. Phys. Chem. B 112 (2008) 5563–5574.
[7] L. Lombardo, S. Brutti, M.A. Navarra, S. Panero, P. Reale, J. Power Sources 227 (2013) 8–14.
[8] S. Swarup, PPG Industries Ohio, Inc. US Patent 8,153,708, 2012.
[9] L.A. Coffey, D.L. Guerchet, L'Oreal US20100074854, WO2008148803A1, 2010.
[10] R. Bernini, E. Mincione, M. Barontini, F. Crisante, G. Fabrizi, A. Gambacorta, Tetrahedron 63 (2007) 6895–6900.
[11] B. Schäffner, J. Holz, S.P. Verevkin, A. Börner, ChemSusChem 1 (2008) 249–253.
[12] B. Schäffner, J. Holz, S.P. Verevkin, A. Börner, Tetrahedron Lett. 49 (2008) 768–771.
[13] J.P. Parrish, R.N. Salvatore, K.W. Jung, Tetrahedron 56 (2000) 8207–8237.
[14] D. Li, W. Fang, Y. Xing, Y. Guo, R. Lin, J. Hazard. Mater. 161 (2009) 1193–1201.
[15] L.R. Rudnick, C. Zecchini, Synthetics, Mineral Oils, and Bio-Based Lubricants: Chemistry and Technology, CRC Press, Boca Raton, FL, 2013, p. 245.
[16] K. Shukla, V.C. Srivastava, Catal. Rev. Sci. Eng. 59 (2017) 1–43.
[17] S. Gryglewicz, F.A. Oko, G. Gryglewicz, Ind. Eng. Chem. Res. 42 (2003) 5007–5010.
[18] a) A.-A.-G. Shaikh, S. Sivaram, Chem. Rev. 96 (1996) 951–976;
b) Y. Ono, Appl. Catal. A 155 (1997) 133–166.
[19] a)H.O. Osaka, H.G. Neyagawa, A.M. Takaishi, US Pat., 5521027, 1996.b) T. W. Greene, P.G. Wuts, J. Wiley, Protective Groups in Organic Synthesis, Wiley, New York, 1999.c)H. Gan, S. Takeuchi, R. Rubino, US Pat., 6759 170, 2004.d)H. Buchold, J. Eberhadt, L. U. Wagner, H. J. Woelk, WO Pat., 2005028415, 2005.e)S. Yukio, T. Masahiro, U. Makoto, JP Pat., 2004010491, 2004.f)M. Miyamoto, T. Tayama, JP Pat., 2005126496, 2005.
[20] a) K.S. Kanakikodi, S.R. Churipard, A.B. Halgeri, S.P. Maradur, Sc. Rep. 10 (2020) 13103;
b) Z. Qi, R. Yan, X. Luo, S. Li, T. Qiu, C. Ye, Langmuir 41 (2025) 23945–23955.
[21] V. Lloret, M. Ángel Rivero-Crespo, J. Alejandro Vidal-Moya, S. Wild, A. Doménech-Carbó, B.S.J. Heller, S. Shin, H.-P. Steinrück, F. Maier, F. Hauke, M. Varela, A. Hirsch, A. Leyva-Pérez, G. Abellán, Nat. Commun. 10 (2019) 509.
[22] H. Pang, G. Yang, L. Li, J. Yu, Green Energ. Environm. 5 (2020) 405–413.
[23] a)Yangzhou Institute of Chemistry and Chemical Engineering, Nanjing University; Jiangsu Oxiran Chemical Co., Ltd. China, CN117567283 A 2024.
[24] a)Zhangjiagang Guotai-Huarong New Chemical Materials Co., Ltd. China, CN1631871A 2005.
b)Qingdao Institute of Bioenergy and Bioprocess Technology, Chinese Academy of Sciences. China, CN109320419A 2019.
c)S. Ge, H. Liu, J. Lyu, J. Liu. Tianjin Haoyong Chemical Eng. Co ltd. CN214088355U 2021.
[25] a)M.H. Lee, J.H. Park, S.H. Kim, S.S. Park. SK Chemicals Co Ltd. WO2006054833A1 2006.b) Z. Zhang, F. Chen, J. Yao, L. Shi, J. Wang, Y. Wang, CN107473968A, Univ. Shenyang Chemical Tech. (2017);
c) L. Shi, J. Fan, G. Xu, W. Deng, J. Liu, Y. Yu, CN109503377A, Univ. Shenyang Chemical Tech. (2019).d)J. B. Park, H. Lee, H. C. Kim. LG Chemical Ltd. WO2023058851A1 2023.
[26] a) S. Jin, A.J. Hunt, J.H. Clark, C.R. McElroy, Green Chem. 18 (2016) 5839–5844;
b) D. Chevella, A.K. Macharla, R. Banothu, K.S. Gajula, V. Amrutham, M. Boosa, N. Nama, Green Chem. 21 (2019) 2938–2945.
[27] a) P. Tundo, F. Trotta, G. Moraglio, F. Ligorati, Ind. Eng. Chem. Res. 27 (1988) 1565–1571;
b) P. Tundo, L. Rossi, A. Loris, J. Org. Chem. 70 (2005) 2219–2224.
[28] a) S. Carloni, D.E. De Vos, P.A. Jacobs, R. Maggi, G. Sartori, R. Sartorio, J. Catal. 205 (2002) 199–204;
b) R.I. Khusnutdinov, N.A. Shchadneva, Y.Y. Mayakova, Russ. J. Org. Chem. 50 (2014) 790–795;
c) F.M. Mei, E.X. Chen, G.X. Li, Kinet. Catal. 50 (2009) 666–670.
[29] a) B. Veldurthy, F. Figueras, Chem. Commun. 6 (2004) 734–735;
b) H. Wang, W. Liu, Y. Wang, N. Tao, H. Cai, J. Liu, J. Lv, Ind. Eng. Chem. Res. 59 (2020) 5591–5600;
c) H. Wang, Y. Wang, W. Liu, H. Cai, J. Lv, J. Liu, Micropor. Mesopor. Mater. 292 (2020) 109757.
[30] X. Zhou, C. Zhang, ACS Omega 6 (2021) 5056–5060.
[31] B. Veldurthy, J.-M. Clacens, F. Figueras, Eur. J. Org. Chem. 2005 (2005) 1972–1976.
[32] T. Wang, X. Li, X. Zhang, J. Dong, Catalysts 11 (2021) 499–519.
[33] a) Y.X. Zhou, S.G. Liang, J.L. Song, T.B. Wu, S.Q. Hu, H.Z. Liu, T. Jiang, B.X. Han, Acta Phys.–Chim. Sin. 26 (2010) 939–945;
b) Z. Qi, S. Li, Y. Cai, R. Cui, J. Chen, C. Ye, T. Qiu, Fuel 334 (2023) 126659.
[34] Y. Zhou, Q. Jin, Z. Gao, H. Guo, H. Zhang, X. Zhou, RSC Adv. 4 (2014) 7013–7018.
[35] a) J. Chen, J. Xie, X. Chen, R. Dong, X.-H. Ge, T. Qiu, Green Chem. 26 (2024) 10500–10511;
b) J. Chen, H. Huang, W. Gong, Y. Chen, R. Dong, L. Ren, T. Qiu, Langmuir 40 (2024) 9233–9243.c)R. Cui, M. Cui, F. Zhang, X. Chen, T. Qiu, J. Chen. Green Chem. Engineer. 2025, in press, doi.org/10.1016/j.gce.2025.11.001.
[36] R. Cui, F. Yin, W. Gong, N. Yan, S. Li, C. Ye, T. Qiu, J. Chen, Green Chem. 27 (2025) 11167–11178.
[37] A. Jia, H. Zhang, J. Zhang, Mol. Catal. 549 (2023) 113505.
[38] a) M. Tejeda-Serrano, M. Mon, B. Ross, F. Gonell, J. Ferrando-Soria, A. Corma, A. Leyva-Pérez, D. Armentano, E. Pardo, J. Am. Chem. Soc. 140 (2018) 8827–8832;
b) M.A. Rivero-Crespo, J. Oliver-Meseguer, K. Kapłońska, P. Kuśtrowski, E. Pardo, J.P. Cerón-Carrasco, A. Leyva-Pérez, Chem. Sci. 11 (2020) 8113–8124;
c) J. Ballesteros-Soberanas, N. Martín, M. Bacic, E. Tiburcio, M. Mon, J. C. Hernández-Garrido, C. Marini, M. Boronat, J. Ferrando-Soria, D. Armentano, E. Pardo, A. Leyva-Pérez, Nat. Catal. 7 (2024) 452–463.
[39] a) I. Zielinska-Nadolska, K. Warmuzinski, J. Richter, Catal. Today 114 (2006) 226–230;
b) P. Rubio-Marques, M.A. Rivero-Crespo, A. Leyva-Perez, A. Corma, J. Am. Chem. Soc. 137 (2015) 11832–11837;
c) F. Garnes-Portolés, R. Greco, J. Oliver-Meseguer, J. Castellanos-Soriano, M. C. Jiménez, M. López-Haro, J.C. Hernández-Garrido, M. Boronat, R. Pérez-Ruiz, A. Leyva-Pérez, Nat. Catal. 4 (2021) 293–303;
d) P. Mingueza-Verdejo, J.C. Hernández-Garrido, A. Vidal-Moya, J. Oliver-Meseguer, A. Leyva-Pérez, Catal. Sci. Technol. 13 (2023) 2308–2316.
[40] a) J.R. Cabrero-Antonino, A. Leyva-Pérez, A. Corma, Angew. Chem. Int. Ed. 54 (2015) 5658–5661;
b) M.Á. Rivero-Crespo, M. Tejeda-Serrano, H. Pérez-Sánchez, J.P. Cerón-Carrasco, A. Leyva-Pérez, Angew. Chem. Int. Ed. 59 (2020) 3846–3849;
c) M. Tejeda Serrano, S. Sanz-Navarro, F. Blake, A. Leyva-Pérez, Synth 52 (2020) 2031–2037.
[41] a) T. Keller, J. Holtbruegge, A. Niesbach, A. Górak, Ind. Eng. Chem. Res. 50 (2011) 11073–11086;
b) T. Keller, J. Holtbruegge, A. Niesbach, A. Górak, Chem. Eng. J. 180 (2012) 309–322.
[42] Y. Guo, R. Wang, C. Shu, H. Li, X. Gao, Sep. Purific. Technol. 338 (2024) 126516.
[43] C. Murugan, H.C. Bajaj, Fuel Process. Technol. 92 (2011) 77–82.
[44] a) Y. Zheng, M. Espinosa, M. Mon, A. Leyva-Pérez, J. Catal. 440 (2024) 115835;
b) P. Mingueza-Verdejo, S. Hervàs-Arnandis, J. Oliver-Meseguer, A. Leyva-Pérez, A.C.S. Org, Inorg. Au 4 (2024) 640–648.
[45] D. Barthomeuf, Stud. Surf. Sci. Catal. 65 (1991) 157–169.
[46] a) R.T. Sanderson, Chemical Bonds and Bond Energy Academic, 2nd ed., Academic Press, New York, 1976;
b) W.J. Mortier, J. Catal. 55 (1978) 138–145;
c) E. Reale, A. Leyva, A. Corma, C. Martínez, H. García, F. Rey, J. Mater. Chem. 15 (2005) 1742–1754;
d) M. Mon, R. Bruno, S. Sanz-Navarro, C. Negro, J. Ferrando-Soria, L. Bartella, L. Di Donna, M. Prejanò, T. Marino, A. Leyva-Pérez, D. Armentano, E. Pardo, Nat. Commun. 11 (2020) 3080;
e) P. Mingueza-Verdejo, D. Velázquez-Ojeda, C. Bilanin, F. Garnes-Portolés, S. Rodríguez-Nuévalos, R. Pérez-Ruiz, J. Oliver-Meseguer, A. Leyva-Pérez, J. Am. Chem. Soc. 147 (2025) 33256–33263.
[47] a) A. Simon, J. Köhler, P. Keller, J. Weitkamp, A. Buchholz, M. Hunger, Micropor. Mesopor. Mater. 68 (2004) 143–150;
b) M.D. Romero, G. Ovejero, A. Rodríguez, J.M. Gómez, Micropor. Mesopor. Mater. 81 (2005) 313–320.

[48] a)F. Klatte, J. Aamodt, D. Biswell, US5776850A, 5, 776, 850, 1998.b) K. Noiroj, P. Intarapong, A. Luengnaruemitchai, S. Jai-In, Renew. Energy 34 (2009) 1145–1150;
c) S. Kosawatthanakun, C. Pansakdanon, N. Sosa, N. Chanlek, F. Roessner, S. Prayoonpokarach, J. Wittayakun, ACS Omega 7 (2022) 9130–9141.
[49] a) J. Lv, H. Cai, Y. Guo, W. Liu, N. Tao, H. Wang, J. Liu, ChemistrySelect 4 (2019) 7366–7370;
b) R. Peña, R. Romero, S.L. Martínez, R. Natividad, A. Ramírez, Fuel 110 (2013) 63–69.
[50] a) Z. Zhang, M. Hu, B. Lv, J. Kang, J. Tang, Z. Fei, X. Chen, Q. Liu, M. Cui, X. Qiao, ACS Omega 3 (2018) 10188–10197;
b) Y. Ha, Y. Park, K. Hyun, S. Lim, M. Choi, Chem. Mater. 36 (2024) 3259–3266.
[51] S. Setiadji, C.D.D. Sundari, V. Aprilia, E. Sumiyanto, I. Novianti, A.L. Ivansyah, J. Phys. Conf. Ser. 1402 (2019) 066016.
[52] a) Y. Zheng, A. Vidal-Moya, J.C. Hernández-Garrido, M. Mon, A. Leyva-Pérez, J. Am. Chem. Soc. 145 (2023) 24736–24745;
b) B. Lerma-Berlanga, F. Orlando, E. Merino, A. Leyva-Pérez, ChemCatChem (2024) e202400909.
[53] a) J.C. Lavalley, Catal. Today 27 (1996) 377–401;
b) H. Knözinger, S. Huber, J. Chem. Soc. Faraday Trans. 94 (1998) 2047–2059;
c) F.X. Llabrés i Xamena, A. Zecchina, Phys. Chem. Chem. Phys. 4 (2002) 1978–1982;
d) G. Martra, R. Ocule, L. Marchese, G. Centi, S. Coluccia, Catal. Today 73 (2002) 83–93;
e) T. Belin, C. Mve Mfoumou, S. Mignard, Y. Pouilloux, Micropor. Mesopor. Mater. 182 (2013) 109–116;
f) H. Bekhti, Y. Boucheffa, A.H. Ait Blal, A. Travert, Vib. Spectrosc. 117 (2021) 103313.
[54] S.Y. Choi, Y.S. Park, S.B. Hong, K.B. Yoon, J. Am. Chem. Soc. 118 (1996) 9377–9386.
[55] a) M.J. Climent, A. Corma, H. Garcia, R. Guil-Lopez, S. Iborra, V. Fornes, J. Catal. 197 (2) (2001) 385–393;
b) L. Xu, X. Wang, Y. Huang, W. Shen, R. Wang, W. Yang, X. Zhang, P. Pan, Y. Yao, ChemistrySelect 10 (2025) e202500844.